EXPERIMENTS ON THE EFFECT OF FREEBOARD ON THE STABILITY OF A BREAKWATER CROWN WALL

Jeroen Bekker[1], Bas Hofland[2] and Gregory Smith[3]

A crown wall is a gravity based structure on top of a rubble mound breakwater which gains stability due to its own weight and friction between the base and contact surface of the rubble mound. An experimental research is carried out in which the global stability of a crown wall is investigated depending on, amongst other things, freeboard. Until now, these structures tend to be designed in a too conservative way, when the vertical distance between base slab and water level (base freeboard) increases. It was concluded that current design methods overpredict vertical loads for increasing freeboard. By implementing a reduction factor for the upward pressure acting on the base slab of the crown wall, a better prediction can be made for the transition region between stability and failure.

Keywords: rubble-mound breakwater; crown wall; freeboard; experimental research; sliding; stability; wave flume; upward pressure; reduction factor.

1. INTRODUCTION

Crown walls are used to increase the breakwater freeboard and to enable transport due to its flat surface. It was expected that the design of these structures, which depends on, amongst other things wave attack, would be too conservative when still water drops below base level of the structure and so the base freeboard R_b increases, see figure 1.

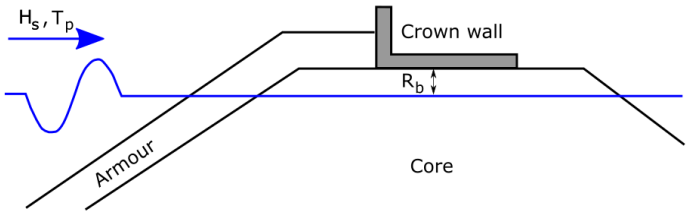

Figure 1: Crown wall on top of rubble mound breakwater.

Therefore this research is focused on the main knowledge gaps with respect to crown wall design. Firstly, little data is available about the effect of varying freeboard with respect to SWL on the stability of the crown wall as function of wave conditions. Secondly, the distribution of the upward pressure against the base slab as a function of freeboard and wave conditions is not sufficiently known. Lastly, insufficient knowledge about a possible phase lag between horizontal and vertical loads as function of freeboard and wave conditions is present.
An experimental research was carried out in a wave flume in the Waterlab of Civil Engineering at Delft University of Technology to investigate the effects of these three aspects on the global stability of a crown wall element.

2. BACKGROUND

Failure mechanisms

To investigate stability of the crown wall it is important to know the possible failure mechanisms of this structure. The most common failure modes can be grouped in those depending on the strength of the structure (such as breakage) and those depending on the interaction with underlying structure (such as sliding and overturning). In this research only the interaction with the underlying rubble

[1] Van Oord Dredging and Marine Contractors, Rotterdam, The Netherlands, jeroen.bekker@vanoord.com
[2] Delft University of Technology & Deltares, Delft, The Netherlands, b.hofland@tudelft.nl
[3] Van Oord Dredging and Marine Contractors, Rotterdam, The Netherlands, greg.smith@vanoord.com

mound material will be considered, and since sliding is the most common failure mechanism according to Pedersen (1996) this will be the only stability criteria considered in this research. Stability is obtained when resistance against sliding is larger than the horizontal force exerted on the crown wall, see figure 2.

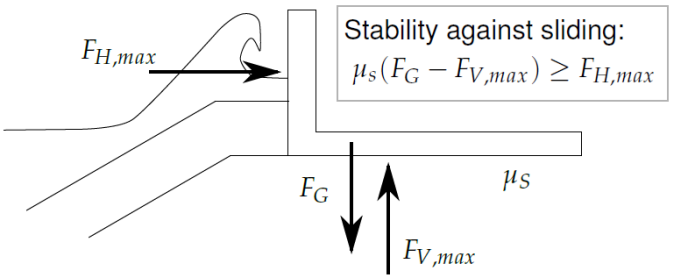

Figure 2: Wave loads on a crown wall.

F_G = (buoyancy-reduced) weight of the crown wall element, = $(M_{cw}\text{-}V_{cw}\ \rho_w)g$, where M_{cw} and V_{cw} are the mass and volume of the crown wall [N/m];
$F_{V,max}$ = wave-induced uplift force [N/m];
$F_{H,max}$ = wave-induced horizontal force [N/m];
μ_s = (static) friction coefficient [-].

Wave load calculation methods

Negro Valdecantos et al. (2013) did a comparative analysis of currently available methods for calculating loads on structures in sloping breakwaters. The aim of this study was to analyse and compare existing wave wall calculation methods of: Iribarren and Nogales (1964), Gűnback and Göcke (1984), Bradbury and Allsop (1988), Pedersen (1996), Martin et al. (1999) and Berenguer and Boanza (2006). Additionally their ranges of application were determined and their uncertainties were detected. Some of the methods indicate their range of validity while others do not. To come to a final design additional tests on a physical model are recommended by Negro Valdecantos et al. (2013). It is stated by Negro Valdecantos et al. (2013), and confirmed by Braña and Gullén (2005), that Martin et al. (1999) gives the best physical insight since it separately analyses the dynamic and quasi-static forces on the structure, whereas Pedersen (1996) is the most reliable method even outside the range of application. For that reason the method of Pedersen (1996) will be investigated within this research. Additionally the method of Pedersen (1996) is extended by Nørgaard et al. (2013) which will be discussed as well.

3. EXPERIMENTAL PROCEDURE

Setup

An experimental research is carried out in which a physical scaled model (1:30) is used. A model of a breakwater is built with on top three crown wall elements which are subjected to wave loads. The tests are performed in the 2-D wave flume in the Waterlab of Civil Engineering & Geosciences at the Delft University of Technology. This flume has an effective length of 42 m, a width of 0.80 m and a height of 1 m. The structure is located at 28 m from the wave generator. A sketch of the set-up is depicted in figure 3.

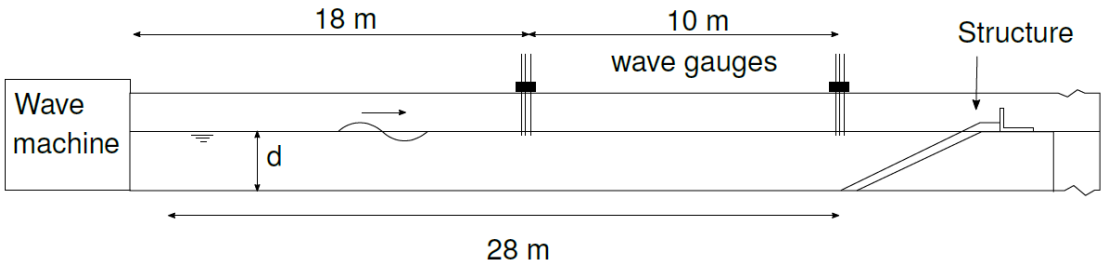

Figure 3: Wave flume setup.

The rubble mound scaled breakwater model existed of a core and armour layer, see figure 4a). Elastocoast was used to bond the rock materials to keep the geometry of the breakwater constant, while the structure remained permeable. Crown walls on top were made of tricoya wood, which hardly deforms (in comparison to other wood species) when it comes in contact with water.
The geometry of the total breakwater was constant during all tests and therefore the freeboard was only varied by changing the water level in the wave flume. On top of the breakwater three crown walls were tested simultaneously in section A, B and C which is shown in figure 4b).

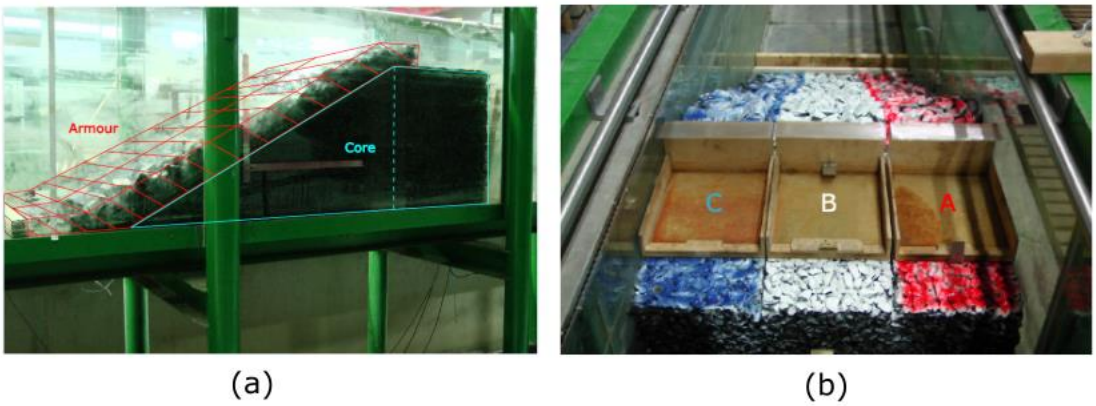

Figure 4: a) Side view of setup of the breakwater in the wave flume. b) Back view in which sections and crown walls are shown.

In figure 5 a simplified setup is given in which the governing parameters and their values or ranges are given. H_s is the significant wave height, T_p the wave peak period, s_{op} the fictitious wave steepness ($=H_s/L_{op}$), h the water depth, d_a the armour layer thickness, B_a the berm width, B_c the base length of the crown wall, W the weight of the crown wall, d_c the crown wall height, R_b the base freeboard, μ_s the static friction coefficient between crown wall and breakwater, $d_{n,50}$ the nominal stone diameter, $d_{n,85}$ / $d_{n,15}$ the grading type, α the structure angle slope and ρ_w the density of water.
The parameters that were varied are: significant wave height, wave peak period, water depth (and hence freeboard), weight of the crown wall and the static friction coefficient between crown wall and breakwater.

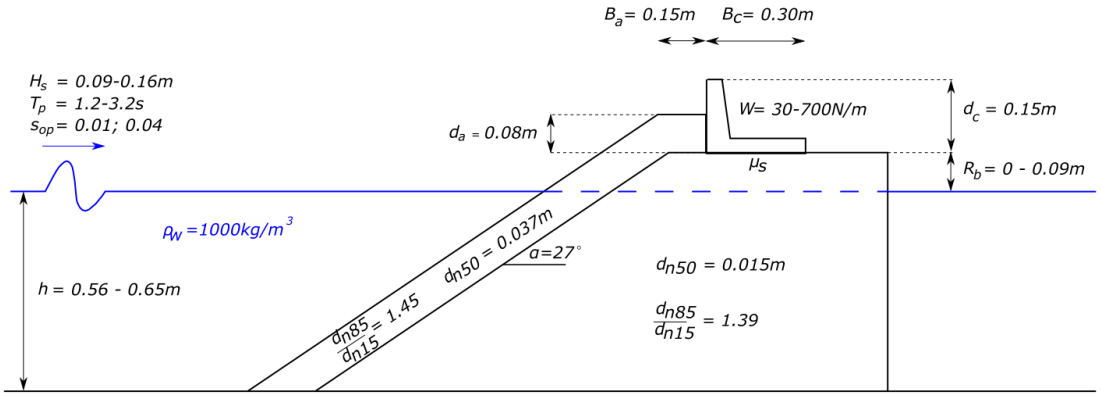

Figure 5: Test parameter range.

Test methods

On top of the breakwater, three parallel test sections were constructed to facilitate testing of three crown wall elements simultaneously. Two test series were devised. In general the test methods concerned sliding of the crown wall, uplifting of the crown wall horizontal and vertical pressures were measured, see figure 6. In total 35 different test conditions were used.

In the first test series, a dataset of critical weights was obtained for several test conditions. The crown wall elements were loaded with different weights, such that iteratively the critical weight for initial displacement (sliding) could be determined. To keep the weight of the crown walls constant during testing, overtopping plates were used to prevent overtopping water from entering the elements, see also figure 7.

For the second test series, the same test conditions were used for pressure measurements and for testing the vertical and overall stability simultaneously.

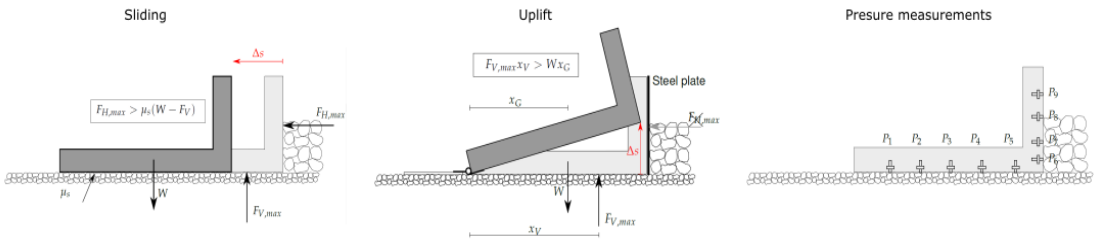

Figure 6: Testing methods in this research - Sliding, uplift and pressure measurements.

The displacement of the crown wall was measured by magnetic rangefinders in a range between 0 - 12 mm with an accuracy of 0.1 mm, see figure 7. The vertical stability was derived according to uplifting in which only vertical displacement was enabled by making use of a hinge on the back of the crown wall fixed to the breakwater, and only exposed to vertical loads since horizontal loads were blocked by an obstruction plate in the middle section, see figure 8. The overall stability was determined in a similar way as in the first test series and used to find a relation between vertical loading at moment of failure.

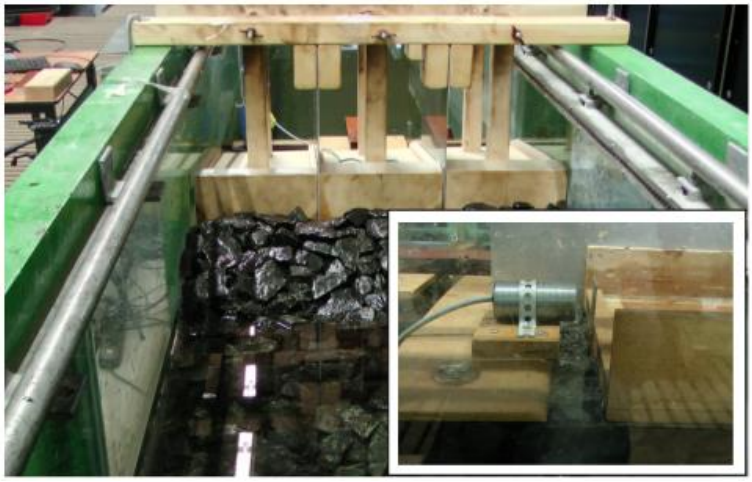

Figure 7: Front view + magnetic range finder - test series 1

Figure 8: Front view of test sections - test series 2

4. RESULTS

General findings

Static friction coefficients, between elements and breakwater, were obtained in both dry and wet conditions for the three different sections, see table 1. A 95% confidence interval is given for an average friction coefficient based on a large number of samples (80) to ensure a precise interval. For section A the highest friction coefficient was found whereas section B had the lowest friction value. It was observed that friction values in wet conditions tend to be higher than in dry conditions. This is most likely due to a sticky/suction effect between the crown wall and core since the structure was permeable. Secondly, the crown walls were fabricated from a softer material (wood) than concrete which is used in practice. It is expected that the rubble mound presses more easily into the wood which increases the friction coefficient as well. According to CIRIA et al. [2007], the friction to be used between a concrete element and rubble mound breakwater is approximately 0.5. However, from an analysis of the damage and repair of Antalya harbour breakwater in Bruun [2013], friction values of 0.7 were measured. In comparison to these values it is concluded that the friction coefficient in this study is somewhat high, which is due to the use of wood in comparison to concrete. The friction is taken into account, according to the formula in figure 2, such that stability is compensated for the higher friction. For the stability analysis the wet friction coefficients are used since failure occurred in wet conditions for each test condition.

Table 1: Static friction values per section for dry and wet conditions

Section	$\mu_{s,dry}$ [-]	$\mu_{s,wet}$ [-]
A	0.70 ± 0.01	0.77 ± 0.01
B	0.67 ± 0.01	0.72 ± 0.01
C	0.69 ± 0.01	0.74 ± 0.01

It is observed that different amounts of overtopping water flew into the three sections, especially for storm waves these differences are relatively large. In figure 9a) this phenomenon is depicted in which the front of the overtopping wave is coloured red. It can be seen that the largest amount of water enters section B followed by C and then A (also observed for regular waves). The same tests have been carried out using a smooth slope (armour was covered by a plate) to ensure an equal geometry over width, see figure 9b). It can be seen that the front line of the entered water is more or less levelled for all three sections. Therefore, it can be concluded that geometry deviations of the armour layer were responsible for differences in the amount of water entering the sections.

From laser measurements average cross sections (95% confidence interval) of the structure per section are obtained based on a sample of 12 measurement strips. These are plotted together in figure 10. It can be seen that cross section A has the highest level whereas cross section B tends to have the lowest structure height at most locations. Since deep water conditions are assumed, inflow differences should especially occur as a result of geometry deviations around the still water level (SWL), which is shown in figure 10. In the lower part of the SWL range the armour of sections A and C is significantly higher than for B (order of magnitude: 1 – 3 cm). Above SWL range the contours of section B and C are more or less equal whereas section A is on average 2 - 3 cm higher. In the last 3 cm of the armour berm, a peak is observed for section C.

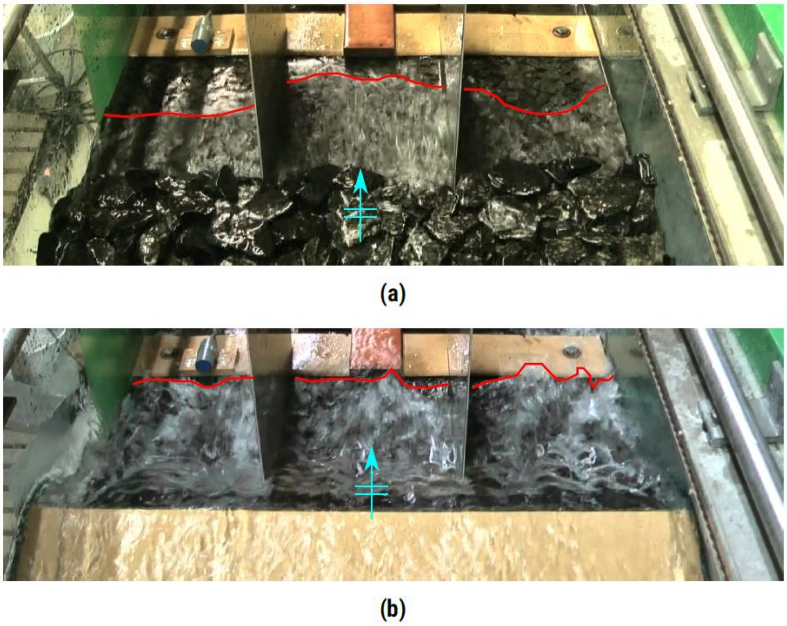

(a)

(b)

Figure 9: Overtopping water impacts a deviating armour layer (a) and a smooth slope (b). Section A on the left, B in the middle and C on the right side in the picture.

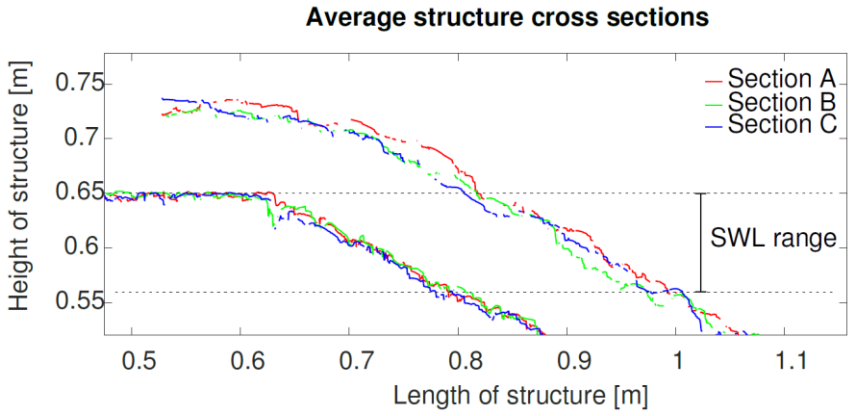

Figure 10: Average cross sections, zooming around SWL.

Upward pressure

It appears that the part of the base which comes in contact with water depends on freeboard. In figure 11 a picture taken from a video record around the moment of failure of the crown wall is shown. Also the corresponding pressure profile can be seen for 4 time steps within this failure interval. From visual analysis it is observed that approximately a maximum of 70% of the base comes in contact with water at the moment of failure, the boundary between contact/no contact is indicated by a red arrow. This location corresponds with the profile where pressure is more or less reduced to 0 at the same location. The same correspondence was found for the other test conditions as well. The covered length is indicated by x_c and the uncovered length is indicated by x_u.

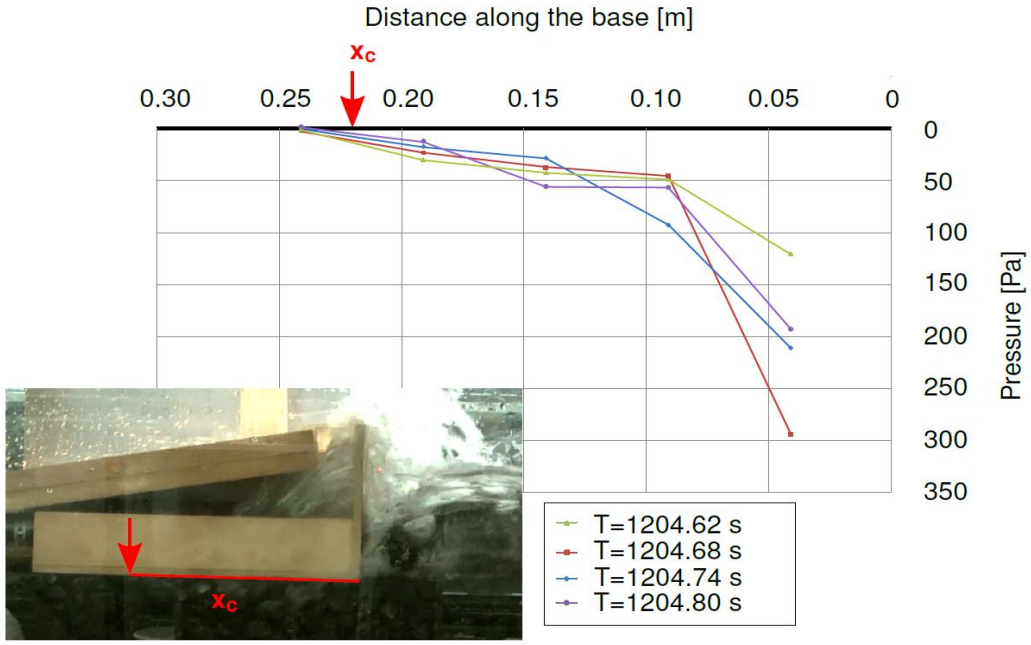

Figure 11: Maximum vertical pressures at three time steps. The distance over which pressure is exerted on the base slab corresponds with the length measured in video analyses.

From pressure measurements it can be concluded that also the shape of the upward pressure varies with varying wave height and freeboard. In figure 9a) and 9b) it is showed that the maximum upward pressure profiles at different time steps in a storm and swell wave series with an effective length equal to the base slab (100% coverage), differ from the currently assumed linear pressure profile by Pedersen (1996) and Nørgaard et al. (2013). Instead, the pressure profile tends to be S-shaped.
However, this shape converts into a polynomial shape if the dimensionless wave height reduces (and hence freeboard increases), see also figure 9c) and 9d).

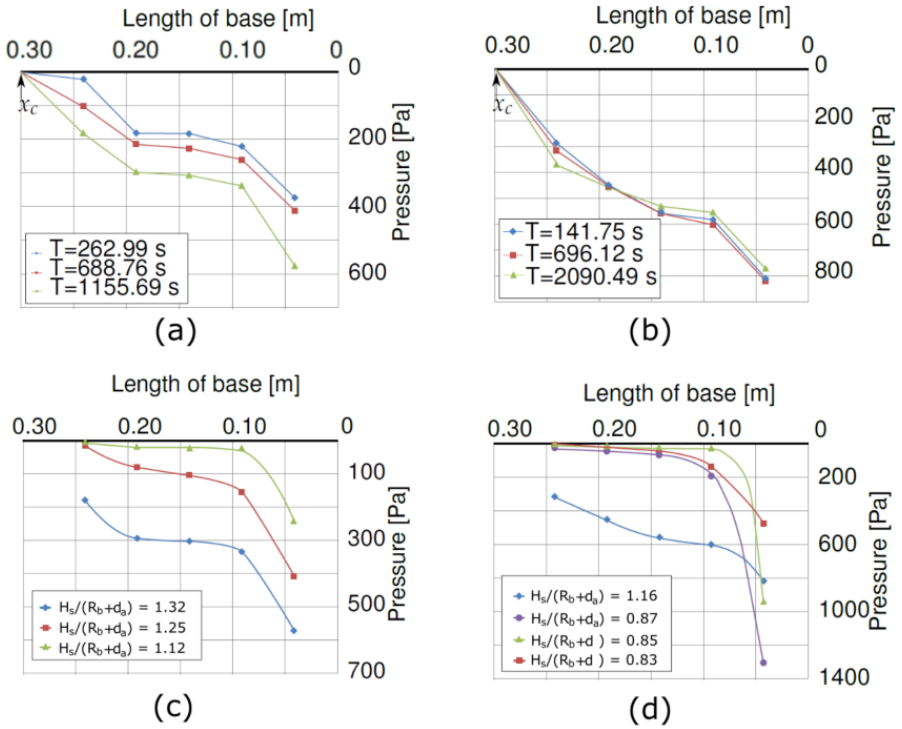

Figure 12: a) Maximum upward pressures in a storm (s_{op}=0.04) wave series. b) Maximum upward pressures in a swell (s_{op}=0.01) wave series. A shape conversion in pressure profile with varying dimensionless wave height for several storm (s_{op}=0.04) wave series c) and swell (s_{op}=0.01) wave series in d).

In figure 13 a summary is given of the shape and effective length belonging to the upward pressure exerting a load on a crown wall when the dimensionless wave height $H_s/(R_b+d_a)$ is large enough. Next to that the currently assumed upward pressure distribution is shown which leads to an overprediction in two ways.

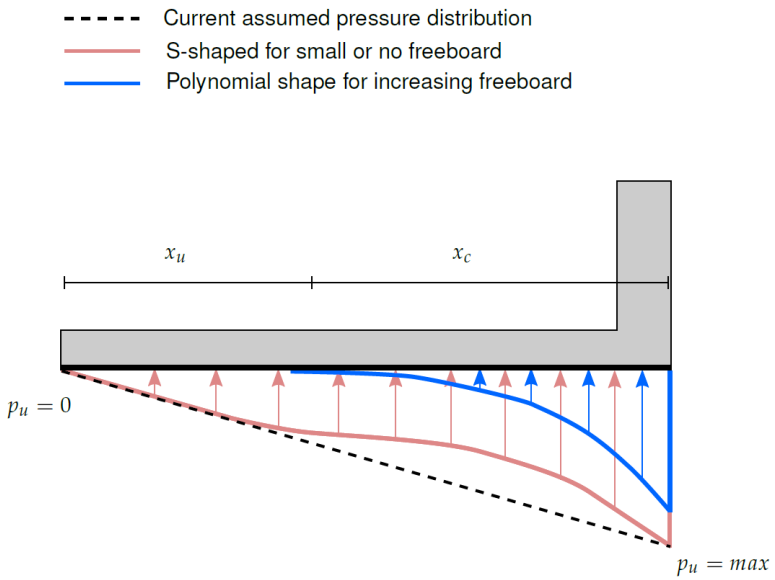

Figure 13: Indication of pressure field under base slab.

Overall stability

Overall stability of the crown wall depends on the resistance against sliding and the loads exerted on the structure. Resistance against sliding is defined as the nett own weight multiplied by the static friction coefficient (which holds during loading conditions): $S = F_G \mu_s$. Loading of the structure takes place due to an interaction between horizontal and vertical loads.

In this research critical weight of the crown wall is defined as: $W_{crit} = mg/\mu_s$, the weight at which the structure is just stable or starts to become unstable (sliding). With m the mass of the crown wall (kg), g the gravitational acceleration (m^2/s) and μ_s static friction coefficient.

In figure 14 data is given of critical weights for the crown wall as function of $H_s^2/(R_b+d_a)^2$ resulting from test series 1. Six different kinds of data points can be distinguished which represent statistical average values of critical weights and corresponding upper- and lower boundaries based on a 95% confidence interval which represents the armour layer differences. Based on linear regression, best fits are drawn through these points. The solid lines give an estimate for the average expected critical weights given a significant wave height and armour crest freeboard. For values of $H_s^2/(R_b+d_a)^2 = 0$ - 0.5 no measurements were done and therefore this extrapolation leads to uncertainties. The best fit for average critical weights considering swell waves crosses the y-axis at y=13.28, which implies that the crown wall should have a weight of 13.28 N/m to be stable while no loading is applied. From a physical point of view this is not correct since zero wave height means the absence of wave load and hence no loads exerted on the crown wall. However, the value of 13.28 N/m is relatively small in comparison to the tangent of the function from which it can be concluded that this physical contradiction can be neglected.

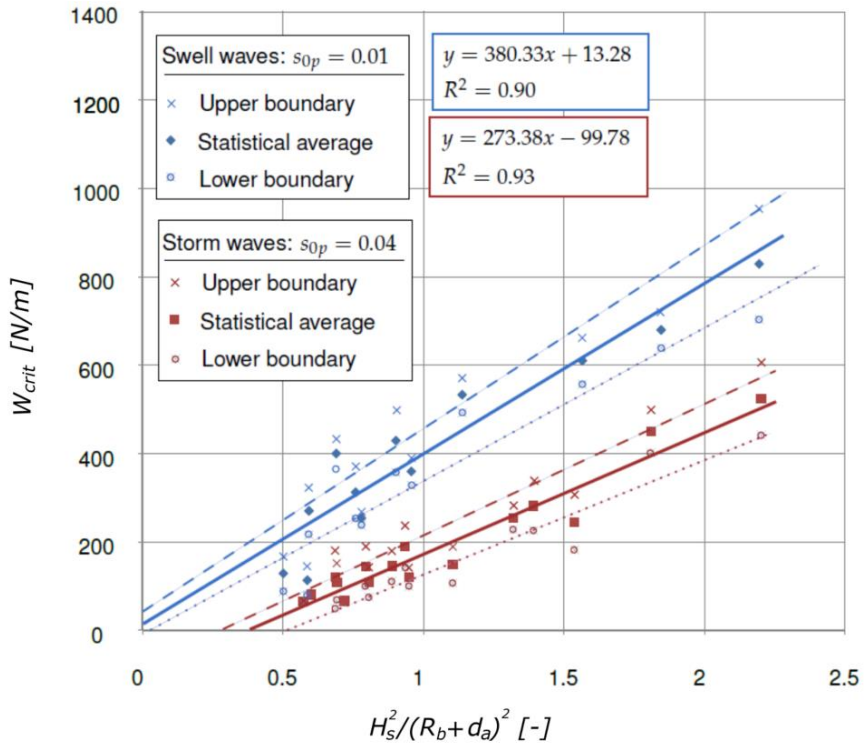

Figure 14: Best fits for critical weights as function of $H_s^2/(R_b+d_a)^2$ for s_{op}=0.01 and s_{op}=0.04.

When the critical weights from figure 14 are compared to the predicted critical weights by using methods of Pedersen (1996) and Nørgaard et al. (2013) for the same wave conditions, it can be seen that for s_{op} = 0.01 Pedersen (1996) is way too conservative in predicting the critical weight especially for increasing freeboard, see figure 15. Nørgaard et al. (2013) proves that his extension approaches the fits better since the overprediction decreases for increasing freeboard in comparison to Pedersen (1996). For larger values of $H_s^2/(R_b+d_a)^2$ (hence decreasing freeboard), Nørgaard et al. (2013) predicts critical weights between the upper- and lower boundaries of the design equations. In the case of s_{op} =

0.04 Pedersen (1996) is still too conservative. However, for low freeboard some critical weights are predicted below the lower boundary of the design equation. Nørgaard et al. (2013) seems to predict the weight better than Pedersen (1996) but also for low freeboard predictions are below the lower boundary of the found fit.
In general, it could be concluded that Nørgaard et al. (2013) provides better predictions than Pedersen (1996) does. Overpredictions tend to increase for increasing freeboard (and hence decreasing $H_s^2/(R_b+d_a)^2$) whereas an decreasing freeboard (hence increasing $H_s^2/(R_b+d_a)^2$) sometimes lead to underprediction of the critical weight with respect to the fit.

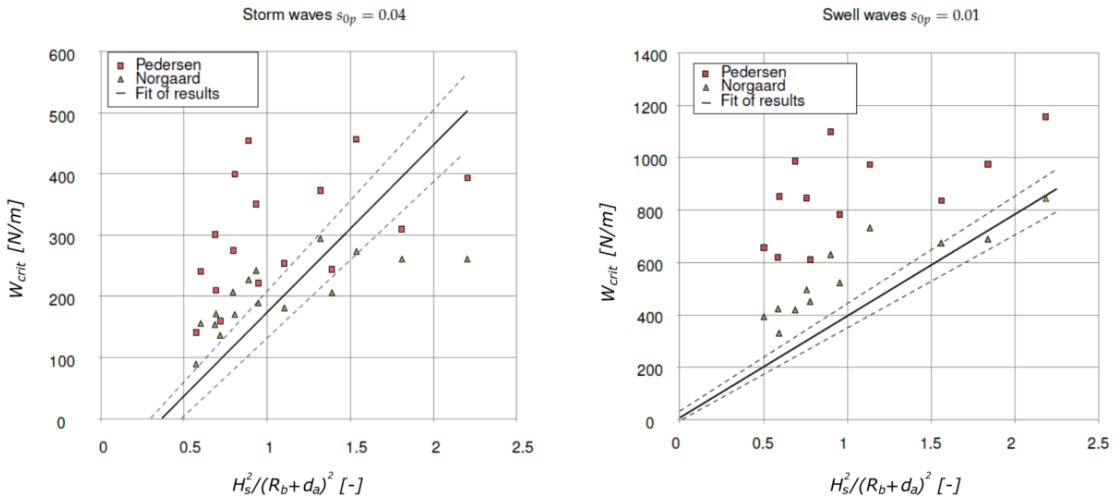

Figure 15: Critical weights by Pedersen (1996) and Nørgaard et al. (2013) compared to the fits of the test results.

Phase lag

To investigate whether phase lag is present between $F_{H,max}$ and $F_{V,max}$, the horizontal and vertical pressure profiles within the failure interval are analysed at several time steps. In figure 16 the vertical and horizontal pressure distribution on the crown wall can be seen for a test condition with storm waves. Through the data points for horizontal pressure a best fit is drawn based on the shape resulting from measurements of Pedersen (1996). The upward pressures at the front side of the base should be equal to the horizontal bottom pressure values since water pressure is isotropic. The effective length, determined by video analysis, is indicated by a red arrow and corresponds to the pressure measurements.
The maximum horizontal pressure occurs at T=273.74 s (red line) whereas the maximum upward pressure occurs 0.11 s later (purple). Based on this, it could be concluded that phase lag is expected to occur, especially for steep waves. For increasing freeboard phase lag could also occur for swell waves.
However, no clear relationships are found and since pressures are filtered quite heavily, this has consequences for the reliability, especially for horizontal measured pressure since these are subjected to dynamic rapidly varying peak loads.

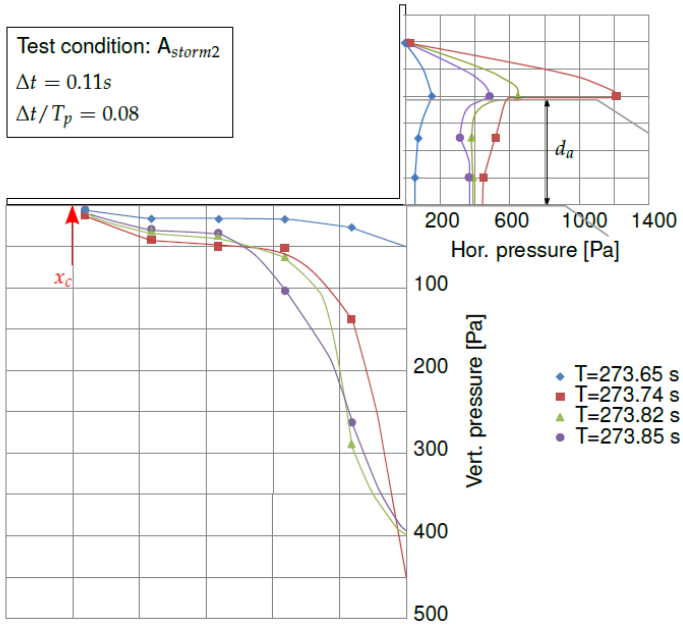

Figure 16: Horizontal and upward pressure profiles for a storm wave condition.

5. ANALYSIS

Reduction coefficient for upward pressure

For every test condition the wet part of the base slab x_c/B_c is presented as a function of dimensionless wave height $H_s/(R_b+d_a)$ for swell- and storm waves which is shown in figure 17. A linear relationship is found for both wave steepness. Reasonable fits were found, with $R^2 = 0.76$ and $R^2 = 0.88$. It can be seen that small values of $H_s/(R_b+d_a)$ (0.60-0.75) lead to an almost negligible effect of upward pressure against the crown wall. When the dimensionless wave height reaches approximately 1.05 or higher for swell waves the base slab comes completely in contact with water and so upward pressure exerts a load over the entire length of the base. For storm waves the threshold lies at a dimensionless wave height of approximately 1.35 or larger.

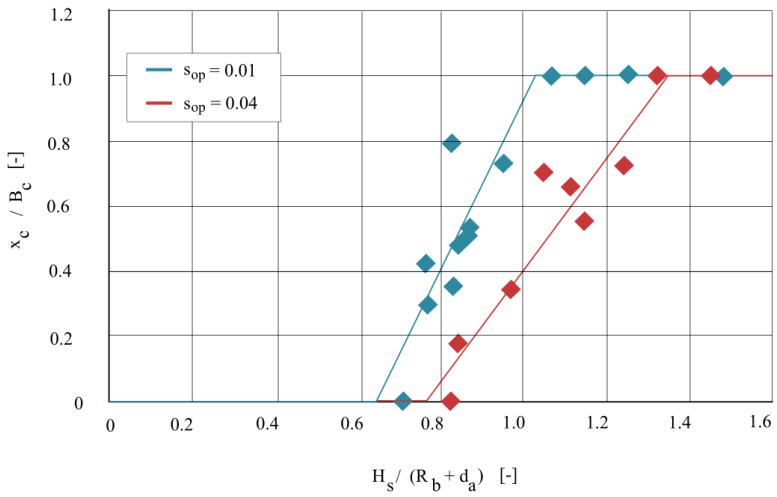

Figure 17: Wet part x_c/B_c of base slab as function of $H_s/(R_b+d_a)$.

Based on the definition of dimensionless contact area between water and the base slab versus a dimensionless wave height a reduction coefficient γ_v, which should be taken into account for vertical load, is defined. This reduction coefficient is described by a set of 3 equations, see below. If the wave is not able to hit the base slab at all $\gamma_v = 0$ (eq. 1), whereas $\gamma_v = 1$ when the base slab is loaded over the full length (eq. 3). In between (eq. 2) holds which is expected to describe γ_v for wave steepness ranging from $s_{op} = 0.01$ till $s_{op} = 0.04$.

(eq. 1) $\gamma_v = 0$ for: $\frac{H_s}{R_b + d_a} < 0.62$

(eq. 2) $\gamma_v = 1.2 \frac{H_s}{R_b + d_a} s_{op}^{-0.14} - 1.44$ for: $0.62 \geq \frac{H_s}{R_b + d_a} \leq 1.30$

(eq. 3) $\gamma_v = 1$ for: $\frac{H_s}{R_b + d_a} > 1.30$

Validation of the reduction coefficient

The reduction coefficient is validated by making use of the collected data with respect to overall stability in combination with adapted methods of Pedersen (1996) and Nørgaard et al. (2013) in which the upward pressure $P_{U,0.1\%}$ is multiplied by γ_v. Doing so, critical weights are determined and plotted together with the obtained critical weights in this research, see figure 18.

It can be seen that for swell waves (s_{op}=0.01) Pedersen (1996) is still too conservative since all the predictions lie outside the confidence interval, whereas Nørgaard et al. (2013) gives results within the upper- and lower boundaries except for some outliers (blue circles and square) which are caused by a substantially larger ratio of $H_{0.1\%}/(R_b+d_a)$ than surrounding points. For storm waves (s_{op}=0.04) most of the predictions by both methods lie within the confidence interval.

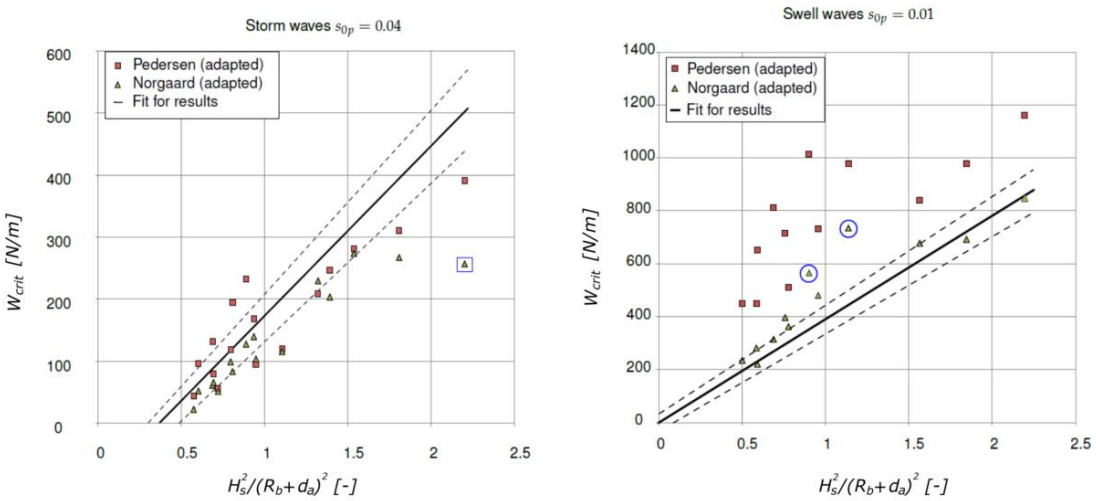

Figure 18: Critical weight predicted by implementing γ_v in methods of Pedersen(1996) and Nørgaard et al. (2013) and compared to the test results.

6. CONCLUSION

In the present experiments, the wave load calculation methods of Pedersen (1996) and Nørgaard et al. (2013) were seen to be conservative in two ways. Firstly, the decrease of effective length x_c over which the upward pressure exerts a load against the base for increasing freeboard is not taken into account. Secondly, the shape of the upward pressure does not follow the previously assumed linear shape. Taking into account this effective length as function of wave height and freeboard in the form of a reduction coefficient γ_v, predictions become substantially better in comparison to the found data set for critical weights. The effect of ignoring highly possible phase lag between horizontal and vertical loads is not as large as supposed at the start of this study.

7. RECOMMENDATIONS

Further research should focus on extending the dataset for critical weights of the crown wall. Adapting the weight of a crown wall until failure occurs is robust since this way of testing always provides useful data. Next to that, is recommended to vary more parameters, which were kept constant in this research, to improve the proposed reduction coefficient and to extent its range of application, see table 2.

Table 2: Range of application.

Parameter	Range
$H_s/(R_b+d_a)$	0.71 - 1.48
H_s/L_{op} (=s_{op})	0.01 ; 0.04
R_b/R_{ca}	0 - 0.53
B_a/d_a	1.88
d_c/d_a	1.88
$d_{n50,c}/d_{n50,a}$	0.40
$(d_{n85}/d_{n15})_c$	1.39
$(d_{n85}/d_{n15})_a$	1.45
cot α	2

For example, the slope of the structure α, the crown wall height d_c and the berm width B_a should be varied. Additionally, it could be useful to extend the dataset for test conditions in which $0.70 > H_s/(R_b+d_a) > 1.50$ since no measurements were done within this range. The pressure sensors which were used during this research have been useful in order to prove that the currently assumed pressure distribution is not correct and to check whether there is a direct relationship between the effective length x_c and pressures. However, because of the known sensitivity for vibrations of the complete system, the records were filtered quite heavily which means that a qualitative analysis is still possible but a quantitative analysis would not be reliable. Therefore, phase lag should be investigated using pressure sensors which are less sensitive for air inclusion and surrounding noise, so that no heavy filters are required. Next to that, heavy filtering could make a phase lag analysis unreliable since relevant peaks are flattened. Secondly, it is desired to measure pressures at the front of the base and at the bottom of the wall. Lastly, it could be sensible to use more sensors to obtain more data.

REFERENCES

Berenguer, J. and Boanza, A. (2006) Rubble mound breakwater crown wall design. *In Proceedings of the National Conference of the Port and Coastal Technical Association*, Algeciras, Spain (in Spanish).

Bradbury, A. and Allsop, N. (1988) P5. Hydraulic effects of breakwater crown walls. *In Design of breakwaters*, Thomas Telford Publishing. 385–396

Braña and Guillén [2005] Wave forces on crown walls: evaluation of existing empirical formulations. *In Coastal Engineering 2004*: (In 4 Volumes),World Scientific. 4087–4099

Bruun, P. (2013) Design and construction of mounds for breakwaters and coastal protection, vol. 37. Elsevier

CIRIA, C. et al. (2007) The rock manual. CIRIA London

Günbak, A. and Gökce, T. (1984) Wave screen stability of rubble-mound breakwaters. *In International symposium of maritime structures in the Mediterranean Sea*. Athens, Greece. 99–112

Martin, F.L., Losada, M.A. and Medina, R. (1999)Wave loads on rubble mound breakwater crown walls. *Coastal Engineering*, 37(2), 149–174

Negro Valdecantos, V., L´opez Gutiérrez, J.S. and Polvorinos Flors, J.I. (2013) Comparative study of breakwater crown wall–calculation methods. *In Proceedings of the Institution of Civil Engineers-Maritime Engineering*. Thomas Telford (ICE Publishing), vol. 166, 25–41

Nørgaard, J.Q.H., Andersen, T.L. and Burcharth, H.F. (2013) Wave loads on rubble mound breakwater crown walls in deep and shallow water wave conditions. *Coastal Engineering*, 80, 137–147

Pedersen, J. (1996) Wave forces and overtopping on crown walls of rubble mound breakwaters. Phd